Tina Memo No. 2004-011
Internal.

Empirical Validation of Cerebrospinal Fluid Pulsatility Model

J. Kim, N.A. Thacker, P.A. Bromiley and A. Jackson.

Last updated
1 / 12 / 2004

Imaging Science and Biomedical Engineering Division,
Medical School, University of Manchester,
Stopford Building, Oxford Road,
Manchester, M13 9PT.

Empirical Validation of Cerebrospinal Fluid Pulsatility Model

J. Kim, N.A. Thacker, P.A. Bromiley and A. Jackson
Imaging Sciences and Biomedical Engineering
The University of Manchester, Manchester M13 9PT, UK
email: {Jieun.Kim; Neil.Thacker}@manchester.ac.uk

Introduction

The brain is surrounded by a rigid skull and an incompressible fluid, CSF (Cerebrospinal Fluid). The pulsatile nature of CSF is induced by systolic inflow and diastolic outflow of blood to/from the brain within each cardiac cycle. The Monro-Kellie doctrine predicts that the CSF pulse will be dissipated by shifting CSF out of the cranial cavity and/or compressing venous structures to eject venous blood flow [27].

In early animal experiments, Bering identified the choroid plexus as a source of CSF production [9] which is identified as bulk flow of CSF. Du Boulay and co-workers confirmed that CSF pulsatility coincide with heart beat [15] which is identified as pulsatile flow of CSF. Pulsatile changes of CSF is related to arterial and venous flow change into the head [19]. It is produced at a rate of $500ml$/day and flows down through the foramen of Monro, down through the aqueduct of Sylvius, and out through the foramen of Lushka and Magendie in the fourth ventricle.

It is widely believed that abnormal behaviour in CSF flow is due to ventricular size, aqueductal diameter, brain compliance, and cerebral blood flow [12]. There are many studies exploring this relationship on healthy subjects and also on patients.

Enzmann and Pelc studied temporal quantitative relationships between blood flow and CSF flow, and concluded from healthy subject studies that the pattern of CSF oscillation through the foramen of Monro and aqueduct confirms that the lateral ventricles, rather than a third ventricular "CSF pump", play the major role in normal CSF flow within the ventricular system [16, 17, 18]. The assumption is that since the brain is not compressible and there is no net CSF flow in or out, volumetric flow capacitance must be provided by a comparable volume of fluid (blood) or tissue displacement [27]. Similar conclusion has been drawn by [3, 10, 11, 22] on control subject studies.

The theory has been further tested and confirmed by studies on patients with various CSF circulatory disorders e.g. hydrocephalus [12, 14, 20, 21, 23, 24, 25, 26, 28, 30, 31], dementia [24, 26], AD (Alzheimer's Disease) [24, 32], especially with hydrocephalus subjects. Hydrocephalus is a condition marked by dilatation of the cerebral ventricles, most often occurring secondarily to obstruction of the CSF pathways and accompanied by an accumulation of CSF within the skull. Patients with this condition have increased aqueductal CSF flow velocity and stroke volume due to enlargement of aqueduct and/or greater systolic inward motion of the ventricles. In some cases of hydrocephalus, the study of before and after VPS (Ventriculoperitoneal Shunting) procedure is of great interest [5, 7, 12, 14, 20, 21, 23].

Bradley and co-workers state that for NPH (Normal Pressure Hydrocephalus), patients with CSF stroke volume greater than $42\mu L$ are likely to respond to VPS ($P < 0.05$). Others [25] also suggested that CSF flow >18ml/min suggests idiopathic NPH and <18ml/min are normal. However this is debatable since reproducibility might be fine but the absolute accuracy of the measurement remains in question and also the sample size is rather small for Bradley study (n=18), and the (Vascular Volume)/(intracranial CSF volume) ratio is reported to be higher in the NPH group than Normals [30, 31], which can be useful for the diagnosis of NPH. Recently, Dixon and co-workers found that there is a lack of significant association between CSF flow at the aqueduct and outcome following VPS. They conclude that although phase-contrast MR measurement of aqueductal CSF flow may be useful in establishing the diagnosis of NPH, CSF flow measurement will play a more limited role in predicting which patients will have a positive response to VPS [14].

Bateman disputed the argument by Bradley and others, arguing that the aqueduct flow is independent of ventricular volume and only dependent on the volume increase of the brain. He argued for venous compression as a cause of NPH [5, 6, 7]. The aqueduct flow is increased in NPH and this may relate to the relative increase in straight sinus pulsation in NPH patients compared with that in healthy subjects, owing to the increased compliance. In NPH, there is significantly reduced craniospinal compliance and, because the CSF flow is also lower than normal,

SSS (superior sagittal sinus) pulsations must be higher than normal to accommodate the arterial pulse. Vascular compliance is decreased in NPH subjects relative to healthy or those with atrophy or arterial ischemia. He suggests that the measuring of compliance markers might be a better indicator of NPH than, say, tap tests or aqueduct flow studies. In a comparison and underlying vascular pathophysiology study behind AD, VD (Vascular Dementia), NPH, Bateman [8] also states that there is an underlying vascular pathophysiology behind conditions of AD, VD, NPH, which is related to the strength of the pulse waves induced in the craniospinal cavity by the arterial vascular tree. It is proposed that the manifestation of the dementia in any one patient is dependant on the way pulsations interact with the brain and its venous and perivascular drainage. This interaction is predominately dependant on the compliance of the craniospinal cavity and the chronicity of the increased pulse wave stress. NPH and ID (Idiopathic Dementia) share reduced venous compliance. However, the practical difference is that in NPH reduced venous compliance would be reversible with shunt insertion while in mixed dementia it would not be. Further studies are needed to test which marker would be better indicator for CSF circulation disorders.

Alperin and co-workers studied relationship between CSF and blood volumetric flow rates and ICP (Intracranial Pressure) at the foramen of magnum and below [1, 2, 13]. They concluded that CNS (Central Nervous System) pulsations below the foramen magnum were effectively driven by the total arteriovenous flow through the skull when the pulsatile flows in different vessels are transduced through a common mechanism and the cervical CNS response is not sensitive to the exact transcranial site of transduction. They included a phantom study as well as a baboon study and demonstrated that there is a linear relationship between MRI (Magnetic Resonance Imaging)-driven and invasive measurements. For NPH, the results show abnormal resistance to the flow of CSF and abnormal brain compliance and they also concluded that CSF movements are driven by pulsations of transcranial blood flow.

MR (Magnetic resonance) technique has been used since the early 90's to study CSF flow [1, 3, 10, 16, 17, 18, 20, 23] and many others, and the protocol appears to be standardised a decade later [25]. Measurement of CSF flow within the cerebral aqueduct is challenging because the diameter of the normal aqueduct is small (1-3mm) and the flow is relatively slow (< 10cm/s). Error is introduced by the partial volume effect of pixels that contain both stationary surroundings and flowing CSF. This error can be reduced if the number of pixels per vessel diameter is maximized and slice thickness is minimized.

In this report, we will investigate the relationship between CSF flow and arterial & venous flow. We devised an electrical equivalent cranial pulsatile model and validate and test the model using MRI data obtained from 12 young healthy controls and 31 elderly with no known CSF abnormalities.

Electric Equivalent CSF Pulsatility Model

The salient biological features we wish to model are shown in Figure 1(a). Narrowed flow paths are expected to have associated impedances and thin boundaries are expected to have compliances which can transmit influence of pressure between fluid pools. The analogy we use to model the biological system into electrical circuit is shown in Figure 1(b).

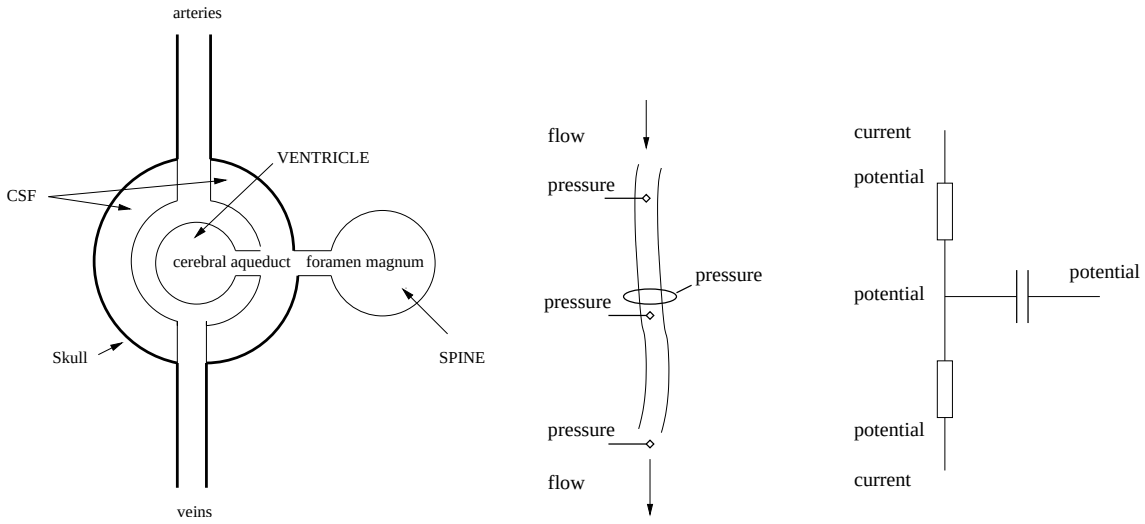

(a) Simplified Biological system

(b) Analogy between current and flow

Figure 1: Biological system and electric current

A full modelling approach would involve a finite element model for a given individual based upon the Navier-Stokes equations, including viscosity terms and elastic tissue boundaries, but we do not have enough measurements to take this approach. The model by Ursino splits the arteries into proximal and distal components (Figure 2 capacitance a) [33]. We may also wish to model compliance between the ventricular and extra-cortical CSF spaces (Figure 2 capacitance c), or compliance of the head (Figure 2 capacitance d). Further refinement might include splitting the arteries to model the effects on the ventricular and extra-cortical compliances separately by including an extra capacitance fed from some point along the artery (Figure 2 capacitance b).

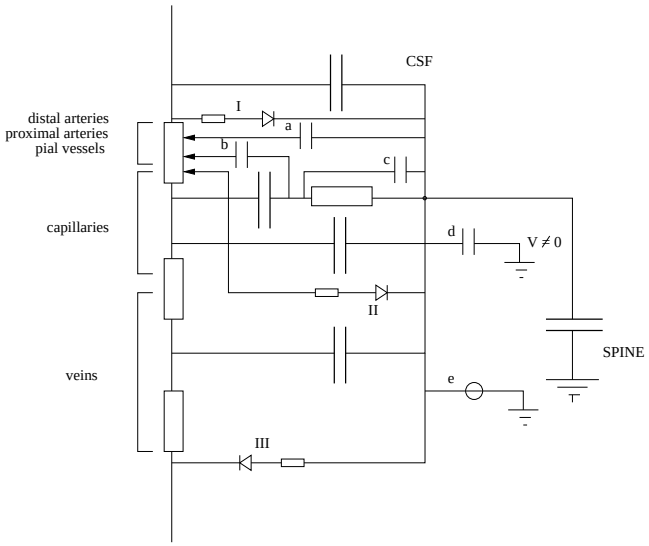

Figure 2: Full electrical circuit.

Assuming for now fixed values for compliances and impedances within this system we can write down an equivalent model as an electrical circuit (Figure 3 (a)). Flow paths with impedance are modelled as resistors and elastic surfaces between any two pressure reservoirs (arteries, brain, veins, CSF, VENTRICLE and SPINE) are modelled as capacitors. Unfortunately some of the components are degenerate so we must combine them to produce a simplified circuit (Figure 3 (b)). As can be seen, this system has 10 free parameters and 6 possible measurements.

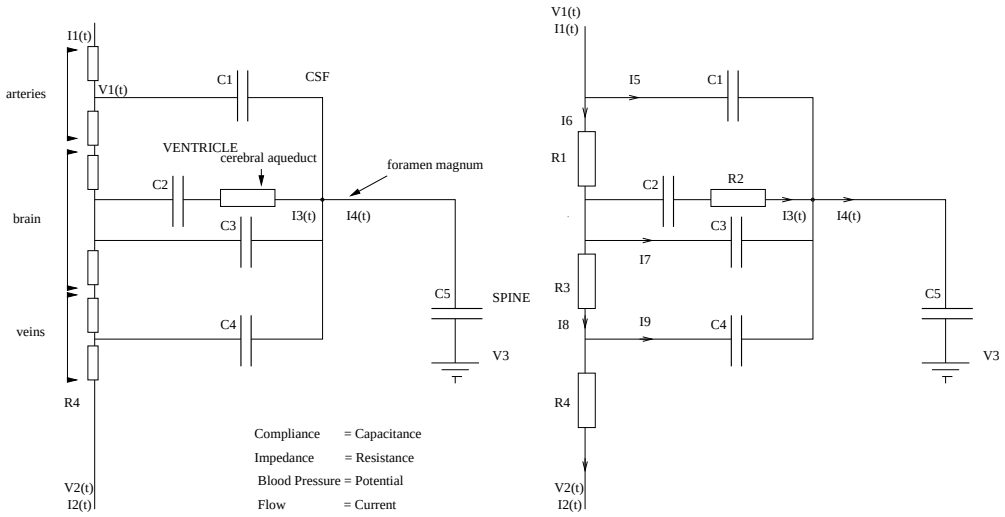

(a) Model for Biological System (b) Equivalent electrical circuit

Figure 3: Electrical Circuits for the Simplified Biological Model.

Analysis of Current Flows

We will assume that we can represent all time varying signals in the Fourier domain so that we can analyse the equivalent circuit at a fixed set of frequencies w. We can then analyse this circuit using conventional means by specifying current flows and writing down the equations describing current and voltage.

Equations we have obtained and detailed analysis is presented in Appendix A. We have obtained the Monro-Kellie Principle which states that whatever goes in must come out, and constraint equation relating currents which does not contain I_1, C_5 or R_4, and scaling equation for variables using mean potentials.

Parameter Estimation

The analysis in Appendix A (though useful as a way of exploring the role of measurements on the parameters) is not sufficient to attempt an optimal estimate of the parameters if we find that we have enough constraints to form an over-determined system. An approach based upon likelihood estimation of parameters is necessary to do that. We can build a suitable likelihood function from Equation (40). By substituting (33) and re-organising terms we can get an equation of the form

$$\gamma I_3 \; - \; \alpha I_1 \; + \; \beta I_4 \; = \; 0 \tag{1}$$

where α, β and γ are complex variables given by;

$$\alpha \; = \; wC_2[C_1R_1 \; - \; C_4R_3]$$

$$\beta \; = \; C_2(wC_1R_1 \; - \; j)$$

$$\gamma \; = \; j(C_1 \; + \; C_2 \; + \; C_3 \; + \; C_4)$$

$$-w[C_2R_2(C_3 \; + \; C_4) \; + \; C_4R_3(C_2 \; + \; C_3) \; + \; C_1(R_1(C_3 \; + \; C_4) \; + \; C_2(R_1 \; + \; R_2) \; + \; C_4R_3)]$$

$$- \; jw^2[C_1C_2R_1R_2(C_3 \; + \; C_4) \; + \; C_4R_3(C_1R_1(C_2 \; + \; C_3) \; + \; C_2R_2(C_1 \; + \; C_3))]$$

$$+ \; w^3C_1C_2C_3C_4R_1R_2R_3$$

The above equation are noise free constraint. Applying the variational method to the constraint Equation (1) we can say that the complex residual on the constraint for each Fourier amplitude w in the measured currents is, Figure 4;

$$F_w \; = \; \gamma I_{3w} \; - \; \alpha I_{1w} \; + \; \beta I_{4w}$$

Assuming equal random independent Gaussian errors (a scalar value) on each of the measured Fourier amplitudes on each current (σ_i) we get the likelihood that we should be minimising in the form of a sum over the appropriate Mahalanobis distance terms from each measured frequency w;

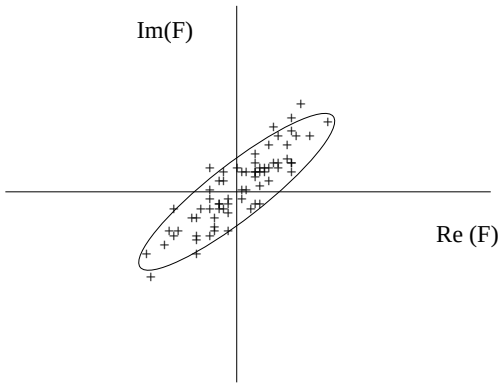

Figure 4: Distribution of measured F for fixed w.

$$-Log(P) \;=\; \sum_w F_w^* F_w / var(F_w) \tag{2}$$

where the variance on the complex residual is given by

$$var(F_w) \;=\; \alpha^*\alpha\ \sigma_1^2 \;+\; \beta^*\beta\ \sigma_4^2 \;+\; \gamma^*\gamma\ \sigma_3^2$$

Box 5: Optimisation Function.

Having determined the most likely parameters for the model we can now make corrections to the flow variables ΔI_n in order to enforce the constraint equations, in a way which minimises the change in measurement consistent with their measurement error.

$$\chi^2 \;=\; \sum_w \Delta I_1^* \Delta I_1/\sigma_1^2 \;+\; \Delta I_3^* \Delta I_3/\sigma_3^2 \;+\; \Delta I_4^* \Delta I_4/\sigma_4^2$$

The minimum of this function at fixed frequency, consistent with the flow constraints [1] is given by:

$$\Delta I_1 \;=\; \frac{\alpha^* F\ \sigma_1^2}{\alpha^*\alpha\ \sigma_1^2 \;+\; \beta^*\beta\ \sigma_4^2 \;+\; \gamma^*\gamma\ \sigma_3^2}$$

$$\Delta I_3 \;=\; \frac{-\gamma^* F\ \sigma_3^2}{\alpha^*\alpha\ \sigma_1^2 \;+\; \beta^*\beta\ \sigma_4^2 \;+\; \gamma^*\gamma\ \sigma_3^2}$$

$$\Delta I_4 \;=\; \frac{-\beta^* F\ \sigma_4^2}{\alpha^*\alpha\ \sigma_1^2 \;+\; \beta^*\beta\ \sigma_4^2 \;+\; \gamma^*\gamma\ \sigma_3^2}$$

Notice that substitution of these equations into the expression for χ^2 above regenerates our earlier expression for $-log(P)$. This suggests that the other way to interpret the parameter estimation process is as direct minimisation of these residual functions.

The final thing we need to know about this result is the expected accuracy of the estimated parameters. If we concatenate the unknown variables in to a 6 dimensional vector $z \;=\; (R_2, R_3, C_1, C_2, C_3, C_4)$, we can write the covariance matrix on the estimated parameters as;

$$Cov(z)^{-1} \;=\; \sum_w \nabla_z F_w Cov(F_w)^{-1} \nabla_z F_w^T$$

which gives us the standard (statistical) errors and correlations on estimated parameters.

[1] Substitute for I_1, differentiate w.r.t. I_3 and I_4 , set the resulting equations to zero and solve.

Image Acquisition and Analysis

The CSF flow at AQ (aqueduct) and FM (foramen of magnum, C2-C3), and blood flow at CAB (carotid & basilar arteries) were studied in 12 young and 31 elderly volunteers (mean age 35.2, 12 male & mean age 74.9, 11 male respectively), and for 22 of them blood flow at SSS was measured as well. Sagittal T1-weighted and PCA (Phase-Contrast Angiogram) scout images were acquired to identify the acquisition level which is perpendicular to the flow we are going to measure, Figure 5 (a) and (b). Within a heart beat, 16 retrospectively cardiac-gated cine phase-contrast MR images are obtained from 1.5T and 3T Phillips medical systems. Image parameters were flip angle 10-15, 5-7mm slice thickness, TR 8.82 - 22.13, and TE 8.14 - 14.39. V_{enc} (velocity encoding) for AQ & FM is set at 10cm/sec, 90cm/sec for CAB, and 40 - 60cm/sec for SSS. Scanning time was depending on subject's heart rate and it usually lasted 2min30sec - 4min for each sequence and makes scanning time for each subject around 30min in total.

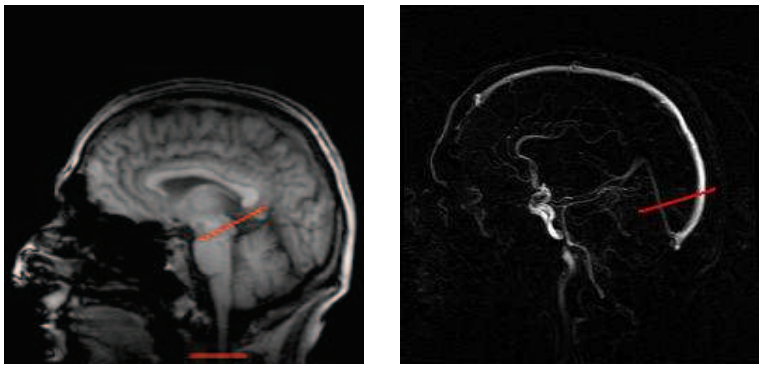

(a) Sagittal T1-weighted MRI (b) PCA MRI

Figure 5: MR Scout Images.

Typical images of a single time point for the measured regions are shown in Figure 6 (a), (b), (c) and (d). Systolic flow will have high intensity value, (a) & (b) and diastolic flow will have low intensity value, (c) & (d). The AQ flow is computed by fitting velocity images in the region over the cerebral aqueduct with a quadratic function and integrating the area under this curve for values of the fitted function above zero. The CAB flow is estimated from the sum of flow values in the foot-to-head direction within the region of the arteries, defined by thresholding the magnitude flow images. The flow into the FM and SSS is obtained in the same way as CAB flow, but in the future FM regions could be automatically located using active shape models.

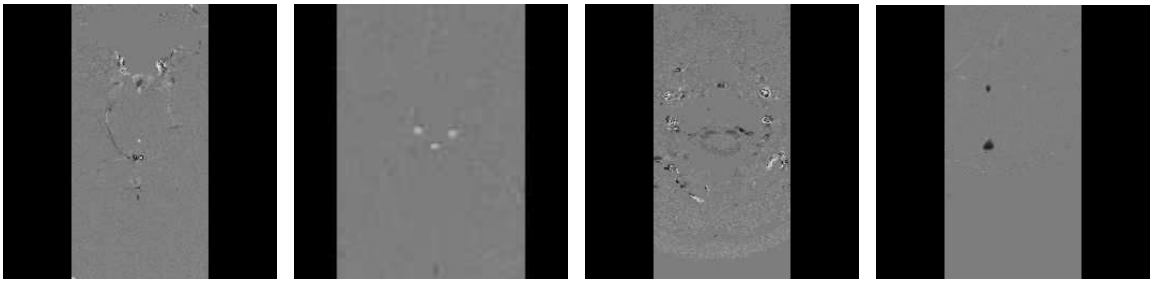

(a) Cerebral Aqueduct. (b) Carotid and Basilar Arteries. (c) Foramen Magnum. (d) Superior Sagittal Sinus.

Figure 6: MR data.

A typical flow graph obtained from each region is presented in Figure 7 for one volunteer. Note that FM flow follows closely to CAB flow and delay between CAB flow and AQ flow.

Results

Table 1 shows flow statistics we obtained from data sets. There are 12 young controls and 31 elderly controls in the set for AQ, CAB, FM data sets, and 11 young controls and 11 elderly controls for SSS data set.

There are no significant differences between young and elderly control subjects in total flow volume for AQ and FM but there is a significant difference in mean total flow in CAB and SSS ($P < 0.05$).

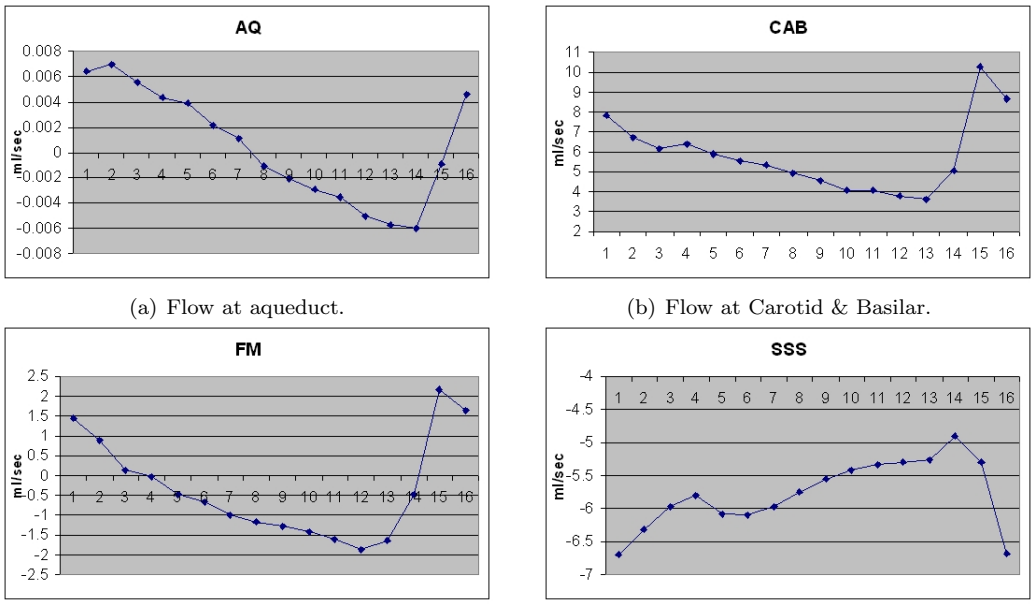

(a) Flow at aqueduct.

(b) Flow at Carotid & Basilar.

(c) Flow at Foramen Magnum.

(d) Flow at Superior Sagittal Sinus.

Figure 7: Flow results.

Region	AQ		CAB		FM		SSS	
Measurements	YC	EC	YC	EC	YC	EC	YC	EC
Total Flow(ml/min)	0.3908	0.3342	689.36	404.30	62.56	55.83	243.99	171.24
Systolic(ml/min)	0.1783	0.1810	689.36	403.42	28.87	34.31	0.0	0.0
Diastolic(ml/min)	0.2125	0.1542	0.0	0.0	33.35	18.18	243.99	171.24

Table 1: Flow results. YC - Young Controls, EC - Elderly Controls.

The approach we would advocate for parameter estimation is as follows. Given measured AQ flow (I_3), FM flow (I_4), and CAB flow (I_1), we minimise Equation (2) as a function of the remaining parameters normalised to any of R_i, because we do not know the scale of variables and also do not know which R_i normalised to. The estimated flows I_3 and I_4 can be corrected back to zero mean.

The results presented here can also be used for modelling. Given the compliances and impedances of the system and the arterial and cerebral aqueduct flow, all other flows and pressures can be computed starting from Equation (1) and working back through the other results. The model could thus be used in a forward manner in order to determine the effects of parameter changes on flow and pressure curves.

Typical input curves are shown in Figure 8 (a) and (b). Repeatability of measurements in a repeated study suggests that the errors on the measured curves are of the order of 0.1 ml/sec for the foramen magnum, 0.15 ml/sec for the arteries and 0.0015 ml/sec for the cerebral aqueduct. These errors are used to scale the fourier terms in Equation (40).

The corrected flow curves (Figure 8(a) and(b)) are consistent within the expected error on the measurement, which implies that the model is adequate to describe the data. The computed flow values at all other points in the model are shown in Figure 8 (c) for one volunteer. Of particular interest are the curves for I_6 and I_8, the flows through intermediate sized blood vessels within the brain. These curves are essentially flat within the expected error, demonstrating that almost all pulsatility has been removed from the arterial input curves, as you would hope for a normal brain. In fact this appears to have come about by shunting the pulsatile component for the arterial input through the foramen magnum. The two curves for these measurements are surprisingly similar.

The median of parameters estimated for the model are given in Table 2. We have normalised parameters to R_1, R_2, and R_3 because we do not know the scale of parameters. The ratio between the computed impedances seems to make sense given the basic geometry of the anatomy. The very small value returned for the elastic capacity of the arteries would seem to imply that this parameter is redundant in normal volunteers.

Fitting parameters by minimising Equation (2) shows that C_1 (arterial capacitance) does not have any effect on

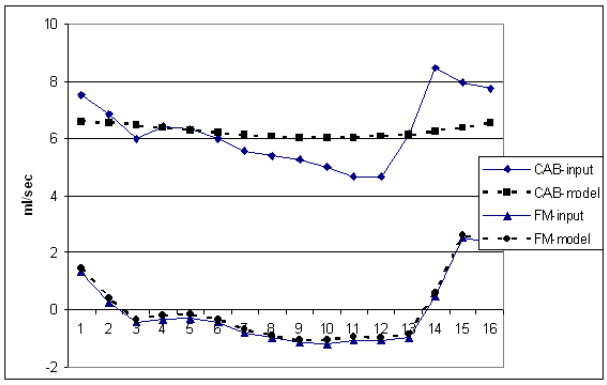

(a) Foramen Magnum and Arteries.

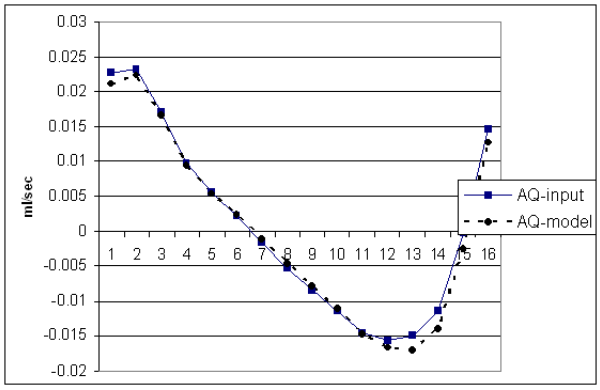

(b) Cerebral Aqueduct .

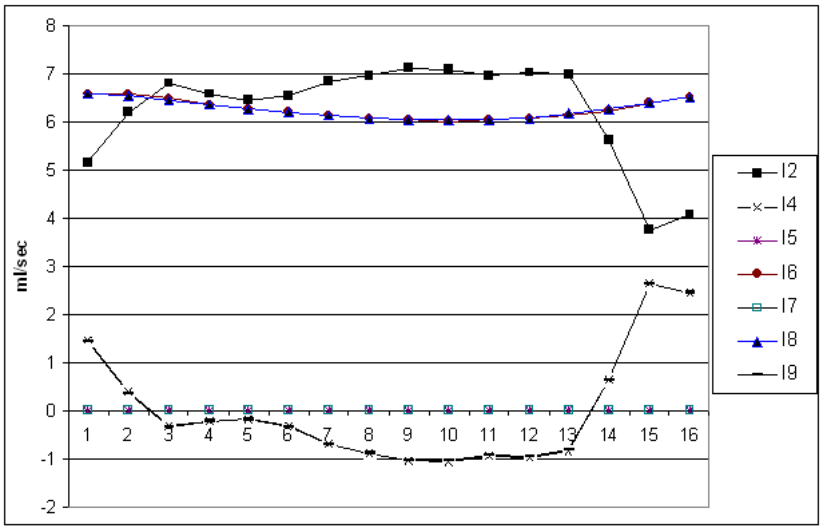

(c) Estimated Flows from model.

Figure 8: Fitted flow data.

Parameter	physical interpretation	R_1	R_2	R_3
R_1	impedance of arterial capillaries	1.0	1522.133	2771.822
R_2	impedance of cerebral aqueduct	0.891369	10.0	0.992421
R_3	impedance of venous capillaries	6.659505	130.9574	1.0
C_1	elastic capacitance of arteries	0.0000275	0.0000495	0.000081
C_2	elastic capacitance of ventricles	0.002366	0.000837	0.000169
C_3	elastic capacitance of capillaries	0.009894	2.341889	0.007855
C_4	elastic capacitance of veins	0.133373	123.0945	0.554642

Table 2: Fitted parameters from a normal subject (arbitrary units).

parameter fitting precess. Figure 9 shows typical fittings of parameters. Throughout the subjects, parameter C_1 shows no effect on overall fitting process. This suggests that whether compliances of arteries are relaxed or not that would not influence pulsatile behaviour of the brain, moreover it would not affect CSF pulsatility.

Although the flow through the cerebral aqueduct is very small, its precision is such that we can still expect useful information regarding the elastic properties of brain tissue and linkage between ventricular and extra-cortical CSF spaces.

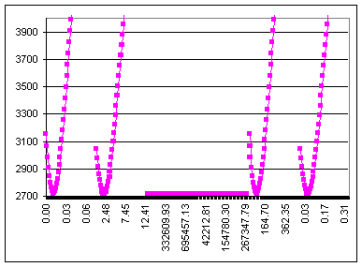

(a) Normalised to R_1. Parameters are in order of R_2 R_3 C_1 C_2 C_3 C_4

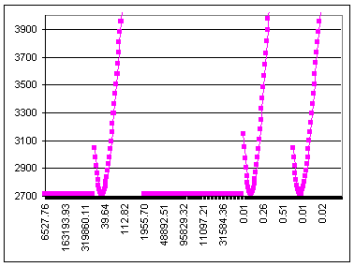

(b) Normalised to R_2. Parameters are in order of R_1 R_3 C_1 C_2 C_3 C_4

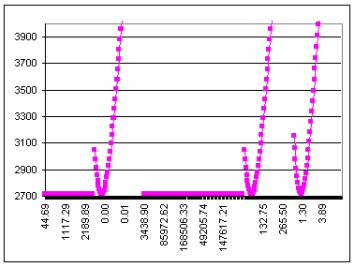

(c) Normalised to R_3. Parameters are in order of R_1 R_2 C_1 C_2 C_3 C_4

Figure 9: Parameter Fittings.

Discussion

According to empirical results shown in this report, we can eliminate (or assume it is so small we can ignore it) parameter C_1 (arterial compliance) and simplify the model accordingly. This will give us the following modified CSF model (Figure 10) and set of simplified equations:

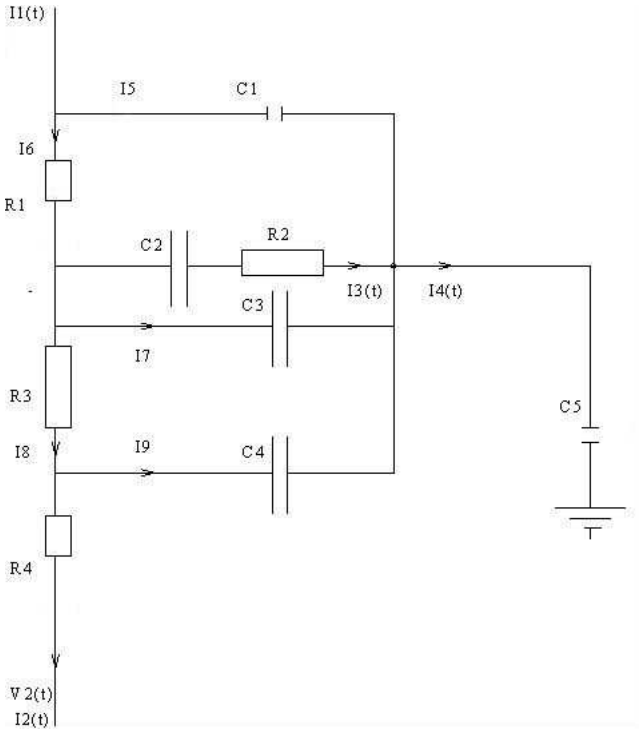

Figure 10: Modified CSF Model.

Vertex Currents

$$I_1 = I_6 \tag{3}$$

$$I_8 = I_9 + I_2 \tag{4}$$

$$I_1 = I_6 = I_3 + I_7 + I_8 \tag{5}$$

$$I_4 = I_3 + I_7 + I_9 \tag{6}$$

Voltage loops

$$I_3 R_2 + I_3 \frac{1}{jwC_2} + I_1 R_1 = 0 \tag{7}$$

$$I_7 \frac{1}{jwC_3} - I_9 \frac{1}{jwC_4} - I_8 R_3 = 0 \tag{8}$$

$$I_3\frac{1}{jwC_2} \; + \; I_3R_2 \; - \; I_7\frac{1}{jwC_3} \; = \; 0 \tag{9}$$

Point to point voltages

$$V_2 - V_1 \; = \; I_1R_1 \; + \; I_8R_3 \; + \; I_2R_4 \tag{10}$$

$$V_3 - V_1 \; = \; I_1R_1 \; + \; I_3\frac{1}{jwC_2} \; + \; I_3R_2 \; + \; I_4\frac{1}{jwC_5} \tag{11}$$

Elimination of Unwanted Variables

Eliminate I_8 using equation (4) from equations (5) and (8);

$$I_1 \; = \; I_3 \; + \; I_7 \; + \; I_9 \; + \; I_2 \tag{12}$$

$$I_7\frac{1}{jwC_3} \; - \; I_9\frac{1}{jwC_4} \; - \; (I_9 \; + \; I_2)R_3 \; = \; 0 \tag{13}$$

Equation (33) stays true.

Eliminate I_9 using (6) from (13) and eliminate I_1 using (33) from (7):

$$I_7\frac{1}{jwC_3} \; - \; (I_4 \; - \; I_3 \; - \; I_7)\frac{1}{jwC_4} \; - \; (I_4 \; - \; I_3 \; - \; I_7 \; + \; I_2)R_3 \; = \; 0 \tag{14}$$

$$-I_3(R_2 - \frac{1}{jwC_2}) \; - \; (I_2 \; + \; I_4)R_1 \; = \; 0 \tag{15}$$

Eliminate I_7 using equation (9) from equations (14) and (15);

$$I_7 \; = \; jwC_3I_3(\frac{1}{jwC_2} \; + \; R_2) \tag{16}$$

giving

$$I_7(\frac{1}{jwC_3} \; + \; \frac{1}{jwC_4} \; + \; R_3) \; - \; (I_4 \; - \; I_3 \;)\frac{1}{jwC_4} \; - \; (I_4 \; - \; I_3 \; + \; I_2)R_3 \; = \; 0 \tag{17}$$

$$jwC_3I_3(\frac{1}{jwC_2} \; + \; R_2)(\frac{1}{jwC_3} \; + \; \frac{1}{jwC_4} \; + \; R_3) \; - \; (I_4 \; - \; I_3)\frac{1}{jwC_4} \; - \; (I_4 \; - \; I_3 \; + \; I_2)R_3 \; = \; 0 \tag{18}$$

Parameter Estimation

$$\gamma I_3 \; - \; \alpha I_1 \; + \; \beta I_4 \; = \; 0 \tag{19}$$

where α, β and γ are complex variables given by;

$$\alpha \; = \; -wC_2C_4R_3 \qquad\qquad \beta \; = \; -jC_2$$

$$\gamma \; = \; j(C_2 \; + \; C_3 \; + \; C_4) - w[C_2R_2(C_3 \; + \; C_4) \; + \; C_4R_3(C_2 \; + \; C_3)] \; - \; jw^2C_2C_3C_4R_2R_3$$

Note that these equations do not include R_1. The optimisation function (2) remains the same.

We have derived a model for CSF pulsatility in the head due to the passage of blood though the brain in one cardiac cycle in the form of an equivalent electrical circuit. This model does not include changes in impedance in arteries and veins. We could use cross-sectional measurement of arteries and veins to try to infer changes in impedance, but this would then prevent the analytic analysis presented here, it would be only possible to write a time stepped simulation. However, as detailed we can infer some conclusions from the above set of equations which (regardless of the simplicity of or model) must be true in general of trying to infer physical flow parameters from the biological model.

Firstly, Equation (33) tells us that once we have measured any two of; arterial flow, venous flow and flow through the foramen magnum, measurement of the third one does not help to constrain directly the model parameters. Though this constraint could be used to improve accuracy of the measurements. However, as detailed agreement between

biology and simplified models is always a difficult issue, it might be more sensible to pick the two measurements thought to be biologically most relevant and not measure the third.

Secondly, the only things which can be measured are arterial compliance, brain compliance, ventricular compliance, venous compliance, arterial impedance, brain impedance and the impedance of the cerebral aqueduct. Even these seven parameters can only be measured up to a scale factor using Equation (40) so we might as well select one and fix it to a nominal value. Thus there are 6 degrees of freedom and we would need constraints at three different frequencies w. This would give enough information to give estimates of the unknown variables by enforcing three (complex) constraint equations.

Finally, we cannot estimate arterial impedance, spine compliance, static pressure or scale the 7 estimated parameters without pressure measurements. As the only other information we can determine from the system would require Equations (27), (28) or (41). In fact the zeroth order term, which corresponds to a relationship between mean arterial flow, mean arterial pressure and mean brain pressure, are enough to establish the scale factor (Equation (42)). Measurements of time dependencies for pressure and flows would however allow additional constraints on the estimation of parameters. A mean head pressure measurement is directly equivalent to V_3 in our model. This means that it should be possible to infer something regarding spine compliance (spinal injury) from mean brain pressure and the time dependencies seen in the arterial flow.

The model identified is the simplest we can manage at this stage and in places, particularly the resistances, it is very difficult to identify specific parts of the anatomy as separable parameters. We would expect all mechanisms relating to net production of CSF to be negligible within a single heart cycle and model-able as a linear function which would have no effect on any non-zero frequency Fourier terms. These processes are however included in the model by Ursino (Figure 2 resistor/diode couplings II and III). Though some production mechanisms (such as from arteries (Figure 2 diode/resistor coupling I) have been neglected. The other major difference between this model and the one presented here is that the equivalent of ventricular and extra-cerebral compliances do not exist in the Ursino model. Instead there is only the equivalent of our spine compliance which Ursino has used for intracranial compliance and (being earthed on one side) has the physical analogy of being set in a vacuum, thus preventing the presence of a non-zero mean pressure in the brain. This has been compensated by the use of a "mock CSF injection rate" (Figure 2 current generator at e), which is not needed in our model.

We have made no attempt to put the relevant dimensions or units on this model for a flow system. We will need to have all of our measurements in a sensible unit scale. Also, we will inevitably find that the equivalence between compliance and capacitance is not straight forward. Compliance is the equivalence of permittivity not capacitance, and to get compliance (the measure of tissue elasticity) we will need scaling variables such as cross-sectional areas and volumes. This means that it will be very difficult to establish expected fixed values which will be valid across different individuals, meaning that all parameters may needed to be determined for everyone for each case in order to gain on unambiguous interpretation of results.

The results obtained from young & elderly volunteers' data suggest that arterial compliance does not have effect on pulsatility of the brain. This contradicts common belief that arterial compliance is a cause of many abnormalities in CSF space [1, 2, 12, 13]. There are several studies on relationship between CSF and arterial waveform and their delays [11, 18]. They found that both arterial and venous waveform amplitude contribute to predicting the CSF waveform amplitude and there is slight delay in CSF flow between the ventricular system and the subarachnoid space. They also suggest that to allow for CSF oscillation there need to be capacitance in the brain system. A portion of this capacitance appears to be in the lumber sac and its associated with the asymmetry in CSF systole and diastole in the spinal subarachnoid space. Obviously this need further investigation to verify it and also if arterial compliance is not a cause of abnormalities in CSF space then we need to find what cause them and how they affect the pulsatile behaviour of CSF in the brain.

References

1. N. J. Alperin, E. M. Vikingstad, et al. Hemodynamically Independent Analysis of Cerebrospinal Fluid and Brain Motion Observed with Dynamic Phase Contrast MRI. *MRM* 35: 741-754, 1962.
2. N. J. Alperin, S. H. Lee, et al. MR-Intracranial Pressure (ICP): A Method to Measure Intracranial Elastance and Pressure Noninvasively by Means of MR Imaging: Baboon and Human Study. *Radiology* 217(3): 877-885, 2000.
3. F. Barkhof, M. Kouwenhoven, et al. Phase-contrast cine MR imaging of normal aqueductal CSF flow. Effect of aging and relation to CSF void on modulus MR. *Acta Radiologica* 35(2): 123-130, 1994.
4. O. Baledent, M. Henry-Feugeas, et al. Cerebrospinal Fluid Dynamics and Relation with Blood Flow: A Magnetic Resonance Study with Semiautomated Cerebrospinal Fluid Segmentation. *Invest. Radiology* 36(7): 368-377, 2001.
5. G. A. Bateman. Vascular Compliance in Normal Pressure Hydrocephalus. *AJNR Am J Neuroradiology* 21: 1574-1585, 2000.

6. G. A. Bateman. Pulse-wave encephalopathy: a comparative study of the hydrodynamics of leukoaraiosis and normal-pressure hydrocephalus. *Neuroradiology* 44: 740-748, 2002.
7. G. A. Bateman. The reversibility of reduced cortical vein compliance in normal pressure hydrocephalus following shunt insertion. *Neuroradiology* 45: 65-70, 2003.
8. G. A. Bateman. Pulse-wave encephalopathy: a spectrum hypothesis incorporating Alzheimer's disease, vascular dementia and normal pressure hydrocephalus. *Medical Hypotheses* 62: 182-187, 2004.
9. E. A. Bering. Circulation of the Cerebrospinal Fluid:Demonstration of the choroid plexuses as the generator of the force for flow of fluid and ventricular enlargement. *J. Neurosurg.* 19: 405-413, 1962.
10. R. A. Bhadelia, A. R. Bogdan, et al. Analysis of Cerebrospinal Fluid Flow Waveforms with Gated Phase-Contrast MR Velocity Measurements. *AJNR Am J Neuroradiology* 16(2): 389-400, 1995.
11. R. A. Bhadelia, A. R. Bogdan, et al. Cerebrospinal fluid pulsation amplitude and its quantitative relationship to cerebral blood flow pulsations: a phase-contrast MR flow imaging study. *Neuroradiology* 39: 258-264, 1997.
12. W. G. Bradley, D. Scalzo, et al. Normal-Pressure Hydrocephalus: Evaluation with Cerebrospinal Fluid Flow Measurements at MR Imaging. *Radiology* 198: 523-529, 1996.
13. D. Chu, D. N. Levin and N. Alperin. Assessment of the Biomechanical state of intracranial tissues by dynamic MRI of cerebrospinal fluid pulsations: A Phantom Study. *Magnetic Resonance Imaging* 16(9): 1043-1048, 1998.
14. G. R. Dixon, J. A. Friedman, et al. Use of Cerebrospinal Fluid Flow rates Measured by Phase-Contrast MR to predict Outcome of Ventriculoperitoneal Shunting for Idiopathic Normal-Pressure Hydrocephalus. *Mayo Clinic Proceedings* 77: 509-514, 2002.
15. G. H. Du Boulay. Further Investigations on Pulsatile Movements in the Cerebrospinal Fluid Pathways. *Acta Radiol Diogn* 13: 497-523, 1972.
16. D. R. Enzmann and N. J. Pelc. Normal flow patterns of intracranial and spinal cerebrospinal fluid defined with phase-contrast cine MR imaging. *Radiology* 178(2): 467-474, 1991.
17. D. R. Enzmann and N. J. Pelc. Brain Motion: Measurement with Phase-Contrast MR Imaging. *Radiology* 185: 653-660, 1992.
18. D. R. Enzmann and N. J. Pelc. Cerebrospinal Fluid Flow Measured by Phase-Contrast Cine MR. *AJNR Am J Neuroradiol* 14(6): 1301-1307; discussion 1309-1310, 1993.
19. D. A. Feinberg and A. S. Mark. Human Brain Motion and Cerebrospinal Fluid Circulation Demonstrated with MR Velocity imaging. *Radiology.* 163: 793-799, 1987.
20. D. Greitz, J. Hannerz, et al. MR imaging of cerebrospinal fluid dynamics in health and disease. On the vascular pathogenesis of communicating hydrocephalus and benign intracranial hypertension. *Acta Radiologica* 35(3): 204-211, 1994.
21. R. Hakim and P.M. Black. Correlation Between Lumbo-Ventricular Perfusion and MRI-CSF Flow Studies in Idiopathic Normal Pressure Hydrocephalus. *Surg. Neurol.* 49: 14-20, 1998.
22. M. Henry-Feugeas, I. IDY-Peretty, et al. Origin of Subarachnoid cerebrospinal fluid pulsations: a phase-contrast MR analysis. *Magnetic Resonance Imaging* 18: 387-395, 2000.
23. D. S. Kim, J. U. Choi, et al. Quantitative assessment of cerebrospinal Fluid hydrodynamics using a phase-contrast cine MR image in hydrocephalus. *Child's Nerv Syst* 15: 461-467, 1999.
24. H. Kitagaki, E. Mori, et al. CSF Spaces in Idiopathic Normal Pressure Hydrocephalus: Morphology and Volumetry. *AJNR Am J Neuroradiology* 19: 1277-1284, 1998.
25. P. H. Luetmer, J. Huston, et al. Measurement of Cerebrospinal Fluid Flow at the Cerebral Aqueduct by Use of Phase-Contrast Magnetic Resonance Imaging: Technique Validation and Utility in Diagnosing Idiopathic Normal Pressure Hydrocephalus. *Neurosurgery* 50(3): 534-543, 2002.
26. T. Miyati, M. Mase, et al. Frequency analyses of CSF flow on cine MRI in normal pressure hydrocephalus. *Eur Radiol* 13: 1019-1024, 2003.
27. B. Mokri. The Monro-Kellie hypothesis: Applications in CSF volume depletion. *Historical Neurology* 56: 1746-1748, 2001.
28. W. R. Nitz, W. G. Bradley, Jr., et al. Flow dynamics of cerebrospinal fluid: assessment with phase-contrast velocity MR imaging performed with retrospective cardiac gating. *Radiology* 183(2): 395-405, 1992.
29. N.A. Thacker and P.A. Bromiley and J. Kim. An Electrical Equivalence Model for CSF Pulsatility. *Tina memo, http://www.tine-vision.net/docs/memos/php*, 2003.
30. A. Tsunoda, H. Mitsuoka, et al. A quantitative index of intracranial cerebrospinal fluid distribution in Normal Pressure hydrocephalus using an MRI-based processing technique. *Neuroradiology* 42: 424-429, 2000.
31. A. Tsunoda, H. Mitsuoka, et al. Intracranial Cerebrospinal Fluid Distribution and its Postoperative Changes in Normal Pressure Hydrocephalus. *Acta Neurochirurgica* 143: 493-499, 2001.
32. S.J. Uftring and D. Chu and others. The mechanical state of intracranial tissues in elderly subjects studied by imaging CSF and brain pulsations. *Magnetic Resonance Imaging* 18: 991-996, 2000.
33. M. Ursino and M. Giulioni. Quantitative Assessment of Cerebral Autoregulation from Transcranial Doppler Pulsatility : a computer simulation study. *Medical Engineering and Physics*, 25:655-666, 2003.

Appendix A

We can then write down the following equations from model Figure 3 (b).

Vertex Currents

$$I_1 = I_5 + I_6 \tag{20}$$
$$I_8 = I_9 + I_2 \tag{21}$$
$$I_6 = I_3 + I_7 + I_8 \tag{22}$$
$$I_4 = I_5 + I_3 + I_7 + I_9 \tag{23}$$

Voltage loops

$$I_5\frac{1}{jwC_1} - I_3R_2 - I_3\frac{1}{jwC_2} - I_6R_1 = 0 \tag{24}$$

$$I_7\frac{1}{jwC_3} - I_9\frac{1}{jwC_4} - I_8R_3 = 0 \tag{25}$$

$$I_3\frac{1}{jwC_2} + I_3R_2 - I_7\frac{1}{jwC_3} = 0 \tag{26}$$

Point to point voltages

$$V_2 - V_1 = I_6R_1 + I_8R_3 + I_2R_4 \tag{27}$$
$$V_3 - V_1 = I_6R_1 + I_3\frac{1}{jwC_2} + I_3R_2 + I_4\frac{1}{jwC_5} \tag{28}$$

We have introduced 5 new current variables (I_5 to I_9), and we have nine equations leaving 6 degrees of freedom.

The point to point voltages require the equivalent of a pressure measurements in the biological system. To begin with we must remove the unmeasured current variables from the (26) remaining constraint equations. This should leave us with two equations composed of variables which are either measured or compliance and impedance parameters of the biological system.

Elimination of Unwanted Variables

In this section we will try to eliminate unwanted variables and produce set of irreducible equations. First, eliminate I_8 using Equation (21) from Equations (22) and (25);

$$I_6 = I_3 + I_7 + I_9 + I_2 \tag{29}$$

$$I_7\frac{1}{jwC_3} - I_9\frac{1}{jwC_4} - (I_9 + I_2)R_3 = 0 \tag{30}$$

Eliminate I_6 using Equation (29) from Equations (20) and (24)

$$I_1 = I_5 + I_3 + I_7 + I_9 + I_2 \tag{31}$$

$$I_5\frac{1}{jwC_1} - I_3(R_2 - \frac{1}{jwC_2}) - (I_3 + I_7 + I_9 + I_2)R_1 = 0 \tag{32}$$

Eliminate I_9 using Equation (31) from Equations (29), (30) and (32);

$$I_1 = I_2 + I_4 \tag{33}$$

Box 1: Monro-Kellie Principle.

This equation is entirely in terms of measured data and is therefore irreducible.

$$I_7\frac{1}{jwC_3} - (I_4 - I_5 - I_3 - I_7)\frac{1}{jwC_4} - (I_4 - I_5 - I_3 - I_7 + I_2)R_3 = 0 \tag{34}$$

$$I_5\frac{1}{jwC_1} - I_3(R_2 - \frac{1}{jwC_2}) - (I_2 + I_4 - I_5)R_1 = 0 \tag{35}$$

Eliminate I_7 using Equation (26) from Equations (34) and (35);

$$I_7 = jwC_3I_3(\frac{1}{jwC_2} + R_2) \tag{36}$$

giving

$$I_7(\frac{1}{jwC_3} + \frac{1}{jwC_4} + R_3) - (I_4 - I_5 - I_3\ )\frac{1}{jwC_4} - (I_4 - I_5 - I_3 + I_2)R_3 = 0 \tag{37}$$

$$jwC_3I_3(\frac{1}{jwC_2} + R_2)(\frac{1}{jwC_3} + \frac{1}{jwC_4} + R_3) - (I_4 - I_5 - I_3 -)\frac{1}{jwC_4} - (I_4 - I_5 - I_3 + I_2)R_3 = 0 \tag{38}$$

Finally rewrite (35) in terms of I_5 and use this in (38) to produce the final irreducible equation.

$$I_5 = \frac{I_3(R_2 + \frac{1}{jwC_2}) + (I_2 + I_4)R_1}{\frac{1}{jwC_1} + R_1} \tag{39}$$

Use $\frac{1}{jwC_n} = D_{nw}$ as shorthand so that all R's are real and all D's imaginary (all I's are complex);

$$(D_{1w} + R_1)[I_3(D_{2w} + R_2)(D_{3w} + D_{4w} + R_3) - D_{3w}(I_4 - I_3\ )D_{4w} - D_{3w}(I_4 - I_3 + I_2)R_3] + D_{3w}[I_3(R_2 + D_{2w}) + (I_2 + I_4)R_1](R_3 + D_{4w}) = 0 \tag{40}$$

Box 2: Constraint equation relating currents (flows).

Notice that this equation does not contain I_1, C_5 or R_4 (though I_1 can be re-introduced using Equation (34)). Thus this equation cannot be used to determine these parameters. In addition there is an overall unknown scale factor leaving a total of 6 degrees of freedom. This constraint equation is complex and therefore provides two constraints for non-zero frequencies. The zeroth order term yields just one equation for the case of $< I_3 > = < I_4 > = 0$ (ie: no net flow out of the ventricles and into the spine) with $< I_2 > \neq 0$ and $D_{3w} \neq 0$.

Using the equations relating point to point voltages

Scaling of parameters will require the use of a point to point voltage equations (such as (27) or (28)). In fact an alternative point to point voltage route gives a simple measurable form immediately.

$$V_3 - V_1 = I_5\frac{1}{jwC_1} + I_4\frac{1}{jwC_5}$$

substituting in (39) and (33) while introducing our shorthand gives

$$V_3 - V_1 = \frac{I_3(R_2 + D_{2w}) + I_1R_1}{D_{1w} + R_1}D_{1w} + I_4D_{5w} \tag{41}$$

Which, again for the mean flow case and $< I_3 > = < I_4 > = 0$ reduces to

$$< V_3 > - < V_1 > = < I_1 > R_1 \tag{42}$$

Box 4: Using mean potentials (pressures) to scale variables.

This suggests that the scaling factor for R_1 (and therefore all of the parameters) can be determined from the zeroth order term. Higher order terms (requiring Fourier terms of $V_1(t)$) provide a constraint on parameter C_5, but do not require additional temporal measurement of V_3, which has been assumed to be static.